Journal of Sound and Vibration 325 (2009) 513–531

Contents lists available at ScienceDirect

Journal of Sound and Vibration

journal homepage: www.elsevier.com/locate/jsvi

Modal analysis of a rotating multi-packet blade system

Ha Seong Lim [a], Jintai Chung [b], Hong Hee Yoo [a,*]

[a] School of Mechanical Engineering, Hanyang University, 17 Haengdang-Dong Sungdong-Gu, Seoul 133-791, South Korea
[b] Department of Mechanical Engineering, Hanyang University, 1271 Sa-1-Dong, Ansan, Kyunggi-Do 425-791, South Korea

ARTICLE INFO

Article history:
Received 23 January 2009
Received in revised form
11 March 2009
Accepted 19 March 2009
Handling Editor: L.G. Tham
Available online 1 May 2009

ABSTRACT

A modeling method for the modal analysis of a multi-packet blade system undergoing rotational motion is presented in this paper. Blades are idealized as tapered cantilever beams that are fixed to a rotating disc. The stiffness coupling effects between blades due to the flexibilities of the disc and the shroud are modeled with discrete springs. Hybrid deformation variables are employed to derive the equations of motion. To obtain more general information, the equations of motion are transformed into a dimensionless form in which dimensionless parameters are identified. The effects of the dimensionless parameters and the number of packets on the modal characteristics of the rotating multi-packet blade system are investigated with numerical examples.

1. Introduction

A rotating multi-blade system can be found in several engineering examples, such as turbine generators, turbo engines, turbo fans, and rotorcraft wings. These structures are comprised of several blades which are attached to a disk and often connected through shrouds. Since the disc and the shroud possess flexibility, they create stiffness coupling effects between blades. The stiffness coupling effect along with the angular motion affects the modal characteristics of the multi-blade system significantly. The modal characteristics of a multi-blade system are different from those of a single blade system. The natural frequencies and the mode shapes of the multi-blade system cannot be accurately predicted by a single blade analysis. To design such a structure properly, therefore, an analysis model for the multi-blade system needs to be developed to estimate the modal characteristics effectively and accurately.

Study on the modal characteristics of a rotating flexible structure originated from the work by Southwell and Gough [1]. They developed a simple analytical model, often called the Southwell equation, to calculate the natural frequencies of a single rotating beam. Schilhansl [2] later derived the partial differential equations of motion for a rotating cantilever beam and applied the Ritz method to obtain more accurate coefficients of the Southwell equation. Since the early 1970s, the fast progress of computing technology has enabled engineers to calculate the modal characteristics of a rotating beam with numerical methods. A large amount of literature related to the subject can be found in two survey papers (see Refs. [3,4]). More recently, the buckling limit as well as the free vibration characteristics was estimated using perturbation techniques (see Ref. [5]). The effect of base translational and rotational motions on the stability of a cantilever beam attached to the base was also studied (see Ref. [6]). To reduce the tip vibration of rotating beam, a control law which employs the shear force measured at the root of the beam was devised (see Ref. [7]) and a piezoelectric actuator was employed to control the vibration of a beam (see Ref. [8]). To derive the equations of motion in a consistent way, a dynamic modeling method employing a set of hybrid deformation variables (see Refs. [9,10]) was introduced. Different from other previous methods in

* Corresponding author. Tel.: +82 2 2220 0446; fax: +82 2 2293 5070.
E-mail addresses: hslim798@hanmail.net (H.S. Lim), jchung@hanyang.ac.kr (J. Chung), hhyoo@hanyang.ac.kr (H.H. Yoo).

0022-460X/$ - see front matter © 2009 Elsevier Ltd. All rights reserved.
doi:10.1016/j.jsv.2009.03.042

which Cartesian deformation variables were only employed, linear equations of motion could be derived directly with the hybrid deformation variable method. The coupling effects between the stretching and the bending motions could be considered (see Ref. [11]) and the modal characteristics of a rotating beam having an arc shape (see Ref. [12]) could be analyzed.

In most of the studies mentioned in the previous paragraph, the modal characteristics of a single blade were only investigated. The study of the modal characteristics of a multi-blade system was presented only in a few papers. The vibration characteristics of stationary coupled turbomachinery blades with various types of connecting elements were calculated by using a transfer matrix method (see Ref. [13]). To obtain the modal characteristics of a rotating multi-blade system, the finite element method could be employed (see, for instance, Ref. [14]). However, if it is employed, the equation size becomes large for a multi-blade system. Such a large size model is not proper for the purpose of system design. It is also not convenient to perform a parameter study with a finite element model. So a simplified model in which blades were idealized as rigid pendulums having discrete torsional springs was employed (see Ref. [15]). More recently, the modal characteristics of rotating disk-blade coupled systems were also investigated (see Ref. [16]).

In this paper, blades are idealized as slender tapered cantilever beams and the stiffness coupling effects between blades due to the flexibilities of the disc and the shroud are modeled with discrete springs. Employing hybrid deformation variables and the Rayleigh–Ritz method, the equations of motion are derived and transformed into a dimensionless parametric form. Even if the equations of motion obtained through the Rayleigh–Ritz method have a relatively small size, they can provide accurate analysis results. Therefore the proposed method is more efficient than the conventional one which employs the finite element method. Furthermore, a parameter study, which is useful for the purpose of system design, can be carried out with the proposed method since the equations of motion are transformed into a dimensionless form.

The purpose of the present study is to propose a dynamic model by which the modal characteristics of a rotating multi-packet blade system can be analyzed efficiently and accurately. Dimensionless parameters are identified with the model so that the effects of the parameters on the modal characteristics of the system can be investigated. As an example of a practical system, a multi-packet blade system having eight packets (a packet has six blades) is chosen. The accuracy and the efficiency of the proposed method need to be verified first through numerical analysis and the effects of the dimensionless parameters related to the disc angular speed, the disc radius, the disc flexibility, the shroud flexibility, the thickness and width taper ratios of the beam cross section, the number of packets and the number of blades per packet are investigated. Since the model proposed in this study is a two-dimensional model, several three-dimensional effects such as pre-twist angle and orientation angles could not be considered in this study. The effects of such angles on the modal characteristics of a single blade were discussed in detail in previous studies (see Refs. [17,18]).

2. Formulation for the modal analysis

Fig. 1 shows the configuration of a multi-packet blade system. The equations of motion of the system are derived based on the following assumptions. All the blades are assumed to have homogeneous and isotropic material properties, and they are idealized as slender beams having tapered rectangular cross section. The variations of width b and thickness h of the cross section are described in Fig. 2. The cross section taper characteristics are described with two dimensionless parameters α and β. If the thickness at the root is h_0, that at the free end is $(1-\alpha)h_0$. Similarly, if the width at the root is b_0 that at the free end is $(1-\beta)b_0$. The shear, the rotary inertia, the eccentricity and the warping effects are not considered in this study. The out-of-plane bending rigidity of the blades is assumed to be much larger than the in-plane bending rigidity. Therefore, only the in-plane bending motions of the blades are considered in this study. The flexibility effects of the disc and the shroud on the stiffness coupling between two blades are considered by using discrete springs.

Fig. 3 shows the configuration of an idealized packet which is connected to other packets. In the figure, $\hat{a}_1$ and $\hat{a}_2$ are unit vectors attached to the rotating disc $\overline{A}$; x is the distance from point O (fixed end of the beam) to point P_0 (the generic point of the kth beam before deformation occurs); k_D and k_S, respectively, are the moduli of the idealized springs due to the disc and the shroud flexibility, respectively; a_D and a_S are the attachment locations of the idealized springs, respectively; and $\vec{u}^{\langle k\rangle}$ and $s^{\langle k\rangle}$ are the elastic deformation vector and the stretch variable of the kth beam, respectively.

The Rayleigh–Ritz assumed mode method is employed to approximate a set of hybrid deformation variables. The stretch variable $s^{\langle k\rangle}$ and the in-plane bending displacement $u_2^{\langle k\rangle}$ can be approximated with mode functions as follows:

$$s^{\langle k\rangle}(x,t)=\sum_{i=1}^{\mu_1}\phi_{1i}(x)q_{1i}^{\langle k\rangle}(t) \tag{1}$$

$$u_2^{\langle k\rangle}(x,t)=\sum_{i=1}^{\mu_2}\phi_{2i}(x)q_{2i}^{\langle k\rangle}(t) \tag{2}$$

where ϕ_{1i} and ϕ_{2i} are the stretching and the bending mode functions of the beam; $q_{1i}^{\langle k\rangle}$ and $q_{2i}^{\langle k\rangle}$ are the corresponding generalized coordinates; and μ_1 and μ_2 are the numbers of the coordinates $q_{1i}^{\langle k\rangle}$ and $q_{2i}^{\langle k\rangle}$, respectively.

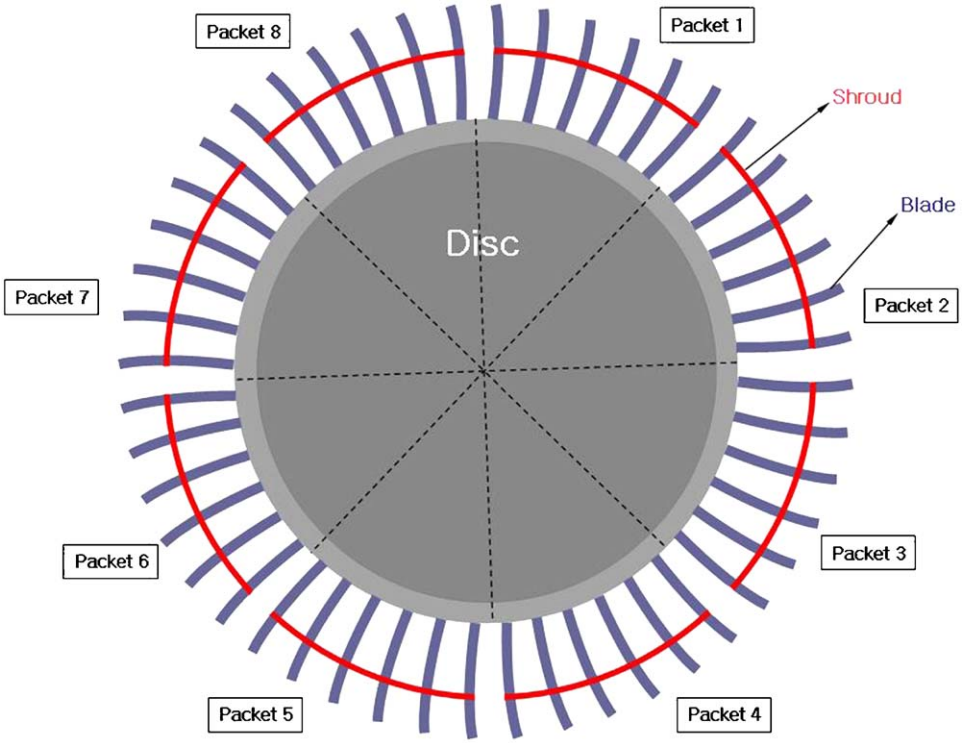

Fig. 1. Configuration of a multi-packet blade system.

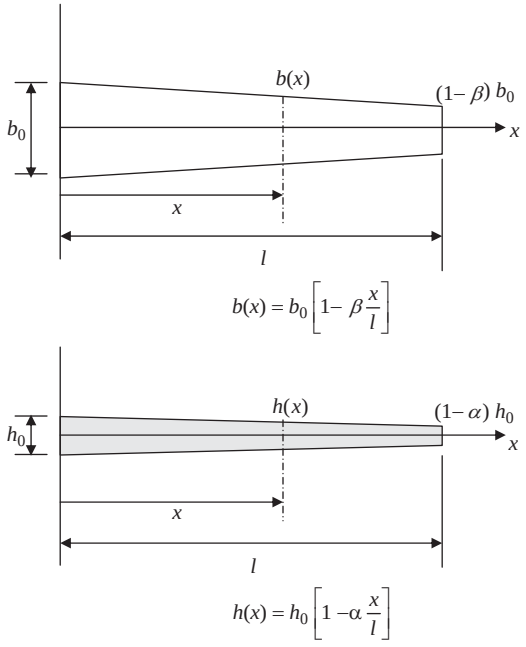

Fig. 2. Variations of the width and thickness of a tapered cross section.

When a disc having radius r rotates with an angular speed Ω, the angular velocity of the disc $\overline{A}$ and the velocity of point P (the generic point after deformation occurs) can be described as follows:

$$\vec{\omega}^{\overline{A}} = \Omega \hat{a}_3 \tag{3}$$

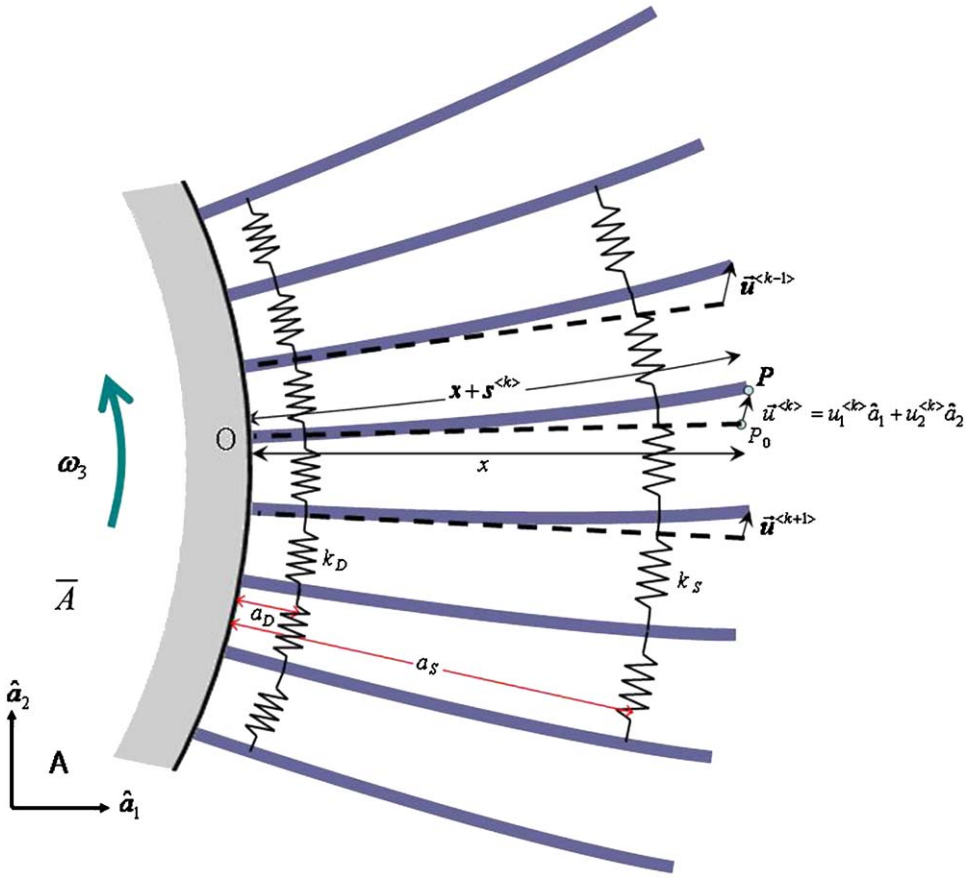

Fig. 3. Configuration of an idealized packet.

$$\vec{v}^P = [\dot{u}_1^{\langle k\rangle} - \Omega u_2^{\langle k\rangle}]\hat{a}_1 + [r\Omega + \dot{u}_2^{\langle k\rangle} + \Omega(x + u_1^{\langle k\rangle})]\hat{a}_2 \tag{4}$$

If Kane's method (see Ref. [19]) is employed, the equations of motion of the kth beam can be derived with the following equation:

$$\int_0^l \rho(x)\left(\frac{\partial \vec{v}^P}{\partial \dot{q}_i}\right)\cdot\frac{\mathrm{d}\vec{v}^P}{\mathrm{d}t}\mathrm{d}x + \frac{\partial U^{\langle k\rangle}}{\partial q_i} = 0 \tag{5}$$

where l is the length, $\rho(x)$ is the mass per unit length, $U^{\langle k\rangle}$ is the strain energy of the beam and q_i's are the generalized coordinates. To obtain $\partial\vec{v}^P/\partial\dot{q}_i$, $\dot{u}_1^{\langle k\rangle}$ in Eq. (4) needs to be expressed with respect to $\dot{s}^{\langle k\rangle}$ and $\dot{u}_2^{\langle k\rangle}$. For the purpose, the following equation can be employed (see Refs. [9–11] in detail).

$$\dot{s}^{\langle k\rangle} = \dot{u}_1^{\langle k\rangle} + \int_0^x \left(\frac{\partial u_2^{\langle k\rangle}}{\partial\sigma}\right)\left(\frac{\partial \dot{u}_2^{\langle k\rangle}}{\partial\sigma}\right)\mathrm{d}\sigma \tag{6}$$

where σ is a dummy variable used for the integration. Now the strain energy of the $\underline{k}$th beam (see Ref. [9]) and the springs attached to the beam can be expressed as follows:

$$\begin{aligned} U^{\langle k\rangle} = {} & \frac{1}{2}\int_0^l \left[EA(x)\left(\frac{\partial s^{\langle k\rangle}}{\partial x}\right)^2 \mathrm{d}x + EI(x)\left(\frac{\partial^2 u_2^{\langle k\rangle}}{\partial x^2}\right)^2 \mathrm{d}x\right] \\ & + \frac{1}{2}k_D[u_2^{\langle k\rangle}(a_D) - u_2^{\langle k-1\rangle}(a_D)]^2 + \frac{1}{2}k_D[u_2^{\langle k+1\rangle}(a_D) - u_2^{\langle k\rangle}(a_D)]^2 \\ & + \frac{1}{2}k_S[u_2^{\langle k\rangle}(a_S) - u_2^{\langle k-1\rangle}(a_S)]^2 + \frac{1}{2}k_S[u_2^{\langle k+1\rangle}(a_S) - u_2^{\langle k\rangle}(a_S)]^2 \end{aligned} \tag{7}$$

where E, $A(x)$ and $I(x)$ are the Young's modulus, the cross-section area and the second area moment of inertia of the cross section, respectively. Since the cross section is tapered, $A(x)$ and $I(x)$ are functions of x. Substituting the strain energy and the kinematic expressions of Eqs. (4), (6) and (7) into Eq. (5), the equations of motion of the kth beam can be derived as

Table 1
Comparison of the first natural frequency of a simple rotating blade with and without the coupling effect between the extensional motion and the bending motion.

δ	γ	Coupling ignored	Coupling included	Error (%)
0	2	3.62	3.62	0
	10	5.05	4.97	1.58
	50	10.5	7.55	28.1
1	2	4.40	4.40	0
	10	13.3	13.1	1.50
	50	61.6	41.4	32.8
5	2	6.65	6.64	0.15
	10	27.7	27.3	1.44
	50	136	74.2	45.4

follows:

$$\sum_{j=1}^{\mu_1}[m_{ij}^{11}\ddot{q}_{1j}^{\langle k\rangle} - \Omega^2 m_{ij}^{11} q_{1j}^{\langle k\rangle} + k_{ij}^{S} q_{1j}^{\langle k\rangle}] - \sum_{j=1}^{\mu_2}[2\Omega m_{ij}^{12}\dot{q}_{2j}^{\langle k\rangle} + \dot{\Omega} m_{ij}^{12} q_{2j}^{\langle k\rangle}] = r\Omega^2 P_{1i} + \Omega^2 Q_{1i} \quad (i = 1, 2, \ldots, \mu_1) \tag{8}$$

$$\begin{aligned}&\sum_{j=1}^{\mu_2}[m_{ij}^{22}\ddot{q}_{2j}^{\langle k\rangle} + \{k_{ij}^{B} + \Omega^2(k_{ij}^{G} - m_{ij}^{22})\}q_{2j}^{\langle k\rangle}] + \sum_{j=1}^{\mu_1}[2\Omega m_{ij}^{21}\dot{q}_{1j}^{\langle k\rangle} + \dot{\Omega} m_{ij}^{21} q_{1j}^{\langle k\rangle}]\\ &\quad - k_{ij}^{Cd}(q_{2j}^{\langle k-1\rangle} - 2q_{2j}^{\langle k\rangle} + q_{2j}^{\langle k+1\rangle}) - k_{ij}^{Cs}(q_{2j}^{\langle k-1\rangle} - 2q_{2j}^{\langle k\rangle} + q_{2j}^{\langle k+1\rangle})\\ &\quad = -r\dot{\Omega}P_{2i} - \dot{\Omega}Q_{2i} \quad (i = 1, 2, \ldots, \mu_2)\end{aligned} \tag{9}$$

where

$$m_{ij}^{ab} = \int_0^l \rho(x)\phi_{ai}(x)\phi_{bj}(x)\,\mathrm{d}x$$

$$k_{ij}^{S} = \int_0^l EA(x)\phi_{1i,x}(x)\phi_{1j,x}(x)\,\mathrm{d}x$$

$$k_{ij}^{B} = \int_0^l EI(x)\phi_{2i,xx}(x)\phi_{2j,xx}(x)\,\mathrm{d}x$$

$$k_{ij}^{G} = \int_0^l G(x)\phi_{2i,x}(x)\phi_{2j,x}(x)\,\mathrm{d}x$$

$$k_{ij}^{Cd} = k_D\phi_{2i}(a_D)\phi_{2j}(a_D)$$

$$k_{ij}^{Cs} = k_S\phi_{2i}(a_S)\phi_{2j}(a_S)$$

$$P_{ai} = \int_0^l \rho(x)\phi_{ai}(x)\,\mathrm{d}x$$

$$Q_{ai} = \int_0^l \rho(x)x\phi_{ai}(x)\,\mathrm{d}x$$

In the above expressions, $\phi_{1i,x}$ and $\phi_{2i,x}$ are the differentiation of the symbols ϕ_{1i} and ϕ_{2i} with respect to x, $\phi_{2i,xx}$ is the double differentiation of the symbol, and a and b are indices which change from 1 to 2. In the definition of the mass matrix element, the mass per unit length ρ is also a function of x since the area of the cross section changes due to the taper effect. In the definition of k_{ij}^{G}, $G(x)$ is also a function of x which can be obtained as follows:

$$G(x) = \rho_0\left[r(l-x) + \frac{[l-(\alpha+\beta)r]}{2l}(l^2 - x^2) + \frac{[r\alpha\beta - l(\alpha+\beta)]}{3l}(l^3 - x^3) + \frac{\alpha\beta}{4l^2}(l^4 - x^4)\right] \tag{11}$$

where ρ_0 is the mass per unit length of the beam at the root.

For beams, the coupling effect between the extensional motion and the bending motion can be usually ignored without losing the accuracy of the modal analysis. Table 1 shows the first natural frequencies of a simple rotating blade obtained with two models: the model of ignoring the coupling effect and the model of including the coupling effect. As shown in the table, the coupling effect does not influence the modal characteristics significantly until the angular speed become very large. Such a high angular speed is, however, seldom employed for most of practical turbine blade systems. So the coupling effect is ignored in this study and the following equation will be employed for the modal analysis. So the bending equation without the coupling terms can be stated as follows:

$$\sum_{j=1}^{\mu_2}[m_{ij}^{22}\ddot{q}_{2j}^{\langle k\rangle}+\{k_{ij}^{B}+\Omega^2(k_{ij}^{G}-m_{ij}^{22})\}q_{2j}^{\langle k\rangle}]-k_{ij}^{Cd}(q_{2j}^{\langle k-1\rangle}-2q_{2j}^{\langle k\rangle}+q_{2j}^{\langle k+1\rangle})$$
$$-k_{ij}^{Cs}(q_{2j}^{\langle k-1\rangle}-2q_{2j}^{\langle k\rangle}+q_{2j}^{\langle k+1\rangle})=0\quad(i=1,2,\ldots,\mu_2) \tag{12}$$

It is useful to rewrite the equations of motion in a dimensionless form and carry out a parameter study. To achieve this, the following dimensionless variables are employed.

$$\tau=\frac{t}{T},\quad \xi=\frac{x}{l},\quad \theta_j^{\langle k\rangle}=\frac{q_{2j}^{\langle k\rangle}}{l} \tag{13}$$

where

$$T=\sqrt{\frac{\rho_0 l^4}{EI_0}}$$

where I_0 is the second area moment of inertia of the cross section at the fixed end. By employing the above dimensionless variables, Eq. (12) can be rewritten as follows:

$$\sum_{j=1}^{\mu_2}[M_{ij}\ddot{\theta}_j^{\langle k\rangle}+\{K_{ij}^{B}+\gamma^2(K_{ij}^{G}-M_{ij})\}\theta_j^{\langle k\rangle}]-K_{ij}^{Cd}(\theta_j^{\langle k-1\rangle}-2\theta_j^{\langle k\rangle}+\theta_j^{\langle k+1\rangle})-K_{ij}^{Cs}(\theta_j^{\langle k-1\rangle}-2\theta_j^{\langle k\rangle}+\theta_j^{\langle k+1\rangle})=0 \tag{14}$$

where $\ddot{\theta}_j^{\langle k\rangle}$ is the double differentiation of $\theta_j^{\langle k\rangle}$ with respect to τ and

$$\gamma=\Omega T$$

$$M_{ij}=\int_0^1(1-\alpha\xi)(1-\beta\xi)\varphi_i(\xi)\varphi_j(\xi)\,\mathrm{d}\xi$$

$$K_{ij}^{B}=\int_0^1(1-\alpha\xi)^3(1-\beta\xi)\varphi_{i,\xi\xi\xi}(\xi)\varphi_{j,\xi\xi\xi}(\xi)\,\mathrm{d}\xi \tag{15}$$

$$K_{ij}^{G}=\frac{1}{2}\int_0^1 g(\xi)\varphi_{i,\xi}(\xi)\varphi_{j,\xi}(\xi)\,\mathrm{d}\xi$$

$$K_{ij}^{Cd}=\beta_D\varphi_i(\xi_D)\varphi_j(\xi_D)$$

$$K_{ij}^{Cs}=\beta_S\varphi_i(\xi_S)\varphi_j(\xi_S)$$

In the above expressions φ_j is a function of ξ which has the same functional value as $\phi_j(x)$, and the additional five dimensionless parameters shown in the expressions are defined as follows:

$$\delta\equiv\frac{r}{l},\quad \beta_D\equiv\frac{k_D l^3}{EI_0},\quad \beta_S\equiv\frac{k_S l^3}{EI_0},\quad \xi_D=\frac{a_D}{l},\quad \xi_S=\frac{a_S}{l} \tag{16}$$

In the definition of K_{ij}^{G}, $g(\xi)$ is given as follows:

$$g(\xi)=\delta(1-\xi)+\tfrac{1}{2}[1-(\alpha+\beta)\delta](1-\xi^2)+\tfrac{1}{3}[\alpha\beta\delta-\alpha-\beta](1-\xi^3)+\tfrac{1}{4}\alpha\beta(1-\xi^4) \tag{17}$$

There is an important point to consider here. Since a shroud does not exist between two packets, no shroud spring stiffness exists between two packets. So Eq. (14) should be modified as follows:

$$\sum_{j=1}^{\mu_2}[M_{ij}\ddot{\theta}_j^{\langle k\rangle}+\{K_{ij}^{B}+\gamma^2(K_{ij}^{G}-M_{ij})\}\theta_j^{\langle k\rangle}]-K_{ij}^{Cd}(\theta_j^{\langle k-1\rangle}-2\theta_j^{\langle k\rangle}+\theta_j^{\langle k+1\rangle})-K_{ij}^{Csf}(\theta_j^{\langle k+1\rangle}-\theta_j^{\langle k\rangle})-K_{ij}^{Csr}(\theta_j^{\langle k-1\rangle}-\theta_j^{\langle k\rangle})=0 \tag{18}$$

where K_{ij}^{Csf} and K_{ij}^{Csr} are defined as follows:

$$K_{ij}^{Csf} \equiv \delta_F^*(k) K_{ij}^{Cs}$$
$$K_{ij}^{Csr} \equiv \delta_R^*(k) K_{ij}^{Cs} \tag{19}$$

In the above equation $\delta_F^*(k)$ and $\delta_R^*(k)$ are defined as follows:

$$\delta_F^*(k) = \begin{cases} 0 & \text{if } mod(k,m) = 0 \\ 1 & \text{otherwise} \end{cases} \tag{20}$$

$$\delta_R^*(k) = \begin{cases} 0 & \text{if } mod(k,m) = 1 \\ 1 & \text{otherwise} \end{cases} \tag{21}$$

where m is the number of blades in a packet and the integer function mod(k,m) is the remnant when k is divided by m. Another point to consider carefully is the numbering of the blades. Since the last blade is connected to the first blade, it should be properly considered in the equations of motion. Suppose that the total number of blades is n. If $k = n$, $k+1$ should be reset as 1 in Eq. (18).

Now by assembling n sets of the equations written in Eq. (18), the total equation can be written as follows:

$$[\overline{M}]\{\ddot{\theta}\} + \langle [\overline{K}] + \gamma^2 \{[\overline{K}^G] - [\overline{M}]\} \rangle \{\theta\} = 0 \tag{22}$$

where

$$[\overline{M}] = \begin{bmatrix} M & 0 & 0 & \bullet & \bullet & \bullet & 0 \\ 0 & M & 0 & & & & \bullet \\ 0 & 0 & M & & & & \bullet \\ \bullet & & & \bullet & & & \bullet \\ \bullet & & & & \bullet & & \bullet \\ \bullet & & & & & \bullet & 0 \\ 0 & \bullet & \bullet & \bullet & \bullet & 0 & M \end{bmatrix} \tag{23}$$

$$[\overline{K}] = \begin{bmatrix} K^B + K^C & -K^{Cd} - K^{Csf} & 0 & 0 & \bullet & \bullet & -K^{Cd} - K^{Csr} \\ -K^{Cd} - K^{Csr} & K^B + K^C & -K^{Cd} - K^{Csf} & 0 & \bullet & \bullet & 0 \\ 0 & -K^{Cd} - K^{Csr} & K^B + K^C & \bullet & \bullet & \bullet & 0 \\ \bullet & 0 & -K^{Cd} - K^{Csr} & \bullet & \bullet & \bullet & \bullet \\ \bullet & \bullet & 0 & \bullet & \bullet & \bullet & 0 \\ 0 & \bullet & \bullet & \bullet & \bullet & \bullet & -K^{Cd} - K^{Csf} \\ -K^{Cd} - K^{Csf} & 0 & 0 & \bullet & 0 & -K^{Cd} - K^{Csr} & K^B + K^C \end{bmatrix} \tag{24}$$

$$[\overline{K}^G] = \begin{bmatrix} K^G & 0 & 0 & \bullet & \bullet & \bullet & 0 \\ 0 & K^G & 0 & & & & \bullet \\ 0 & 0 & K^G & & & & \bullet \\ \bullet & & & \bullet & & & \bullet \\ \bullet & & & & \bullet & & \bullet \\ \bullet & & & & & \bullet & 0 \\ 0 & \bullet & \bullet & \bullet & \bullet & 0 & K^G \end{bmatrix} \tag{25}$$

$$\{\theta\} = \begin{Bmatrix} \theta^{\langle 1 \rangle} \\ \theta^{\langle 2 \rangle} \\ \bullet \\ \bullet \\ \bullet \\ \theta^{\langle n-1 \rangle} \\ \theta^{\langle n \rangle} \end{Bmatrix} \tag{26}$$

Table 2
Comparison of modal analysis results obtained with the present method and a commercial finite element code.

Mode	$\alpha = 0$		$\alpha = 0.5$	
	$\beta = 0$	$\beta = 0.5$	$\beta = 0$	$\beta = 0.5$
1st	4.074	4.525	4.845	5.305
	4.047	*4.494*	*4.812*	*5.268*
2nd	5.032	5.300	5.838	6.087
	5.003	*5.269*	*5.804*	*6.050*
3rd	5.032	5.300	5.838	6.087
	5.003	*5.269*	*5.804*	*6.050*
4th	5.135	5.368	5.935	6.151
	5.102	*5.334*	*5.897*	*6.110*
5th	5.135	5.368	5.935	6.151
	5.102	*5.334*	*5.897*	*6.110*
6th	5.155	5.381	5.954	6.163
	5.122	*5.346*	*5.916*	*6.122*
7th	5.155	5.381	5.954	6.163
	5.122	*5.346*	*5.916*	*6.122*
8th	5.159	5.384	5.958	6.166
	5.125	*5.349*	*5.919*	*6.124*
9th	6.145	6.951	7.392	8.394
	6.113	*6.914*	*7.353*	*8.349*
10th	6.145	6.951	7.392	8.394
	6.113	*6.914*	*7.361*	*8.358*
11th	6.145	6.951	7.392	8.394
	6.119	*6.922*	*7.361*	*8.358*
12th	6.145	6.951	7.392	8.394
	6.120	*6.922*	*7.362*	*8.359*

($\gamma = 5$, $\delta = 0$, $\beta_D = 2E6$, $\beta_S = 10$, $\xi_D = 0.1$, $\xi_S = 1.0$).
Roman: Present; Italic: ANSYS.

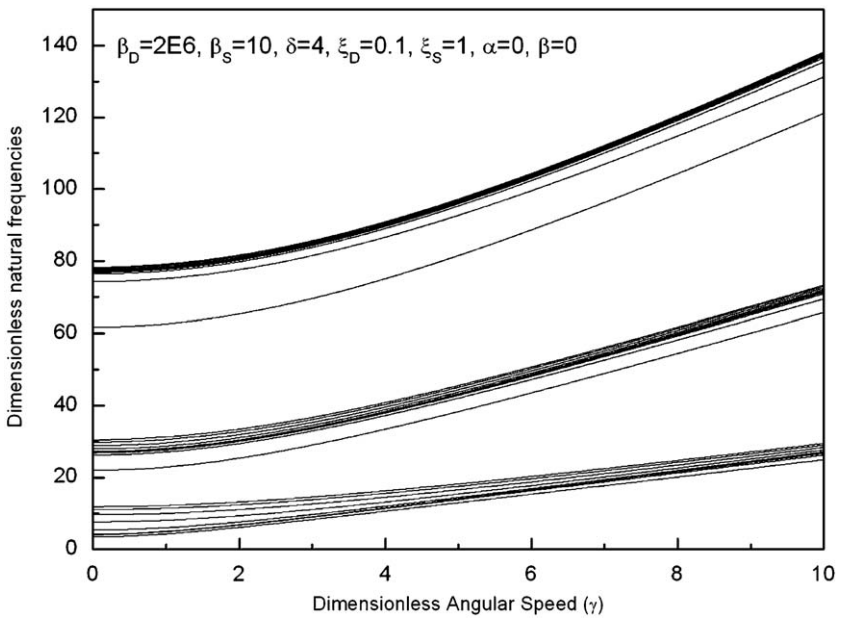

Fig. 4. Three sets of natural frequencies versus the angular speed.

In the above expression K^C is defined as follows:

$$K^C = 2K^{Cd} + K_{ij}^{Csf} + K_{ij}^{Csr} \tag{27}$$

Even if the stiffness matrix $[\overline{K}]$ shown in Eq. (24) looks asymmetric, it is actually symmetric. If Eqs. (20) and (21) are applied, $[\overline{K}]$ can be expressed as follows:

$$[\overline{K}] = \begin{bmatrix} K^B + K^C & -K^{Cd} - K^{Cs} & 0 & 0 & \bullet & \bullet & -K^{Cd} \\ -K^{Cd} - K^{Cs} & K^B + K^C & -K^{Cd} - K^{Cs} & 0 & \bullet & \bullet & 0 \\ 0 & -K^{Cd} - K^{Cs} & K^B + K^C & \bullet & \bullet & \bullet & 0 \\ \bullet & 0 & -K^{Cd} - K^{Cs} & \bullet & \bullet & \bullet & \bullet \\ \bullet & \bullet & 0 & \bullet & \bullet & \bullet & 0 \\ 0 & \bullet & \bullet & \bullet & \bullet & \bullet & -K^{Cd} - K^{Cs} \\ -K^{Cd} & 0 & 0 & \bullet & 0 & -K^{Cd} - K^{Cs} & K^B + K^C \end{bmatrix} \tag{28}$$

Now for the modal analysis of the system, the column matrix $\{\theta\}$ can be expressed as follows:

$$\{\theta\} = e^{j\omega\tau}\{\eta\} \tag{29}$$

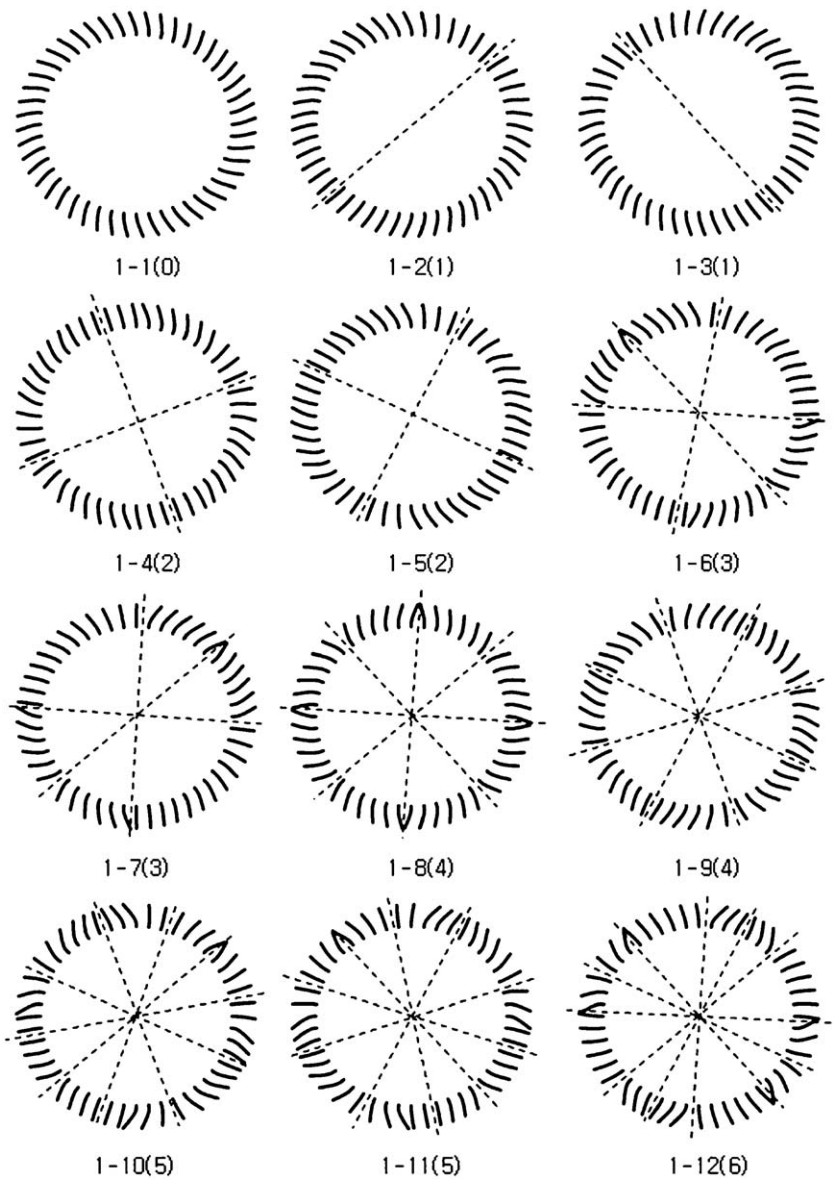

Fig. 5. The lowest 12 mode shapes of the first set of natural frequencies.

where ω is the dimensionless natural frequency of the system. Substituting Eq. (29) into Eq. (22), the following equation can be obtained.

$$\omega^2[\overline{M}]\{\eta\} = \langle[\overline{K}] + \gamma^2\{[\overline{K}^G] - [\overline{M}]\}\rangle\{\eta\} \tag{30}$$

Eq. (30) is employed for the modal analysis of the multi-packet blade system in the following section.

In this study, the extensional deflection is not considered. However, it could be an important factor since it can creates a rub-induced vibration which is another source of dynamic instability (see Refs. [20–24]) such as short time impulse, periodic pulse loadings, and flow induced loadings. If the extensional deflection exceeds the tip-clearance, it can create such vibration phenomena. With the coupled equations of motion presented in this study, such phenomena can be investigated effectively. In this study, however, such phenomena are not investigated.

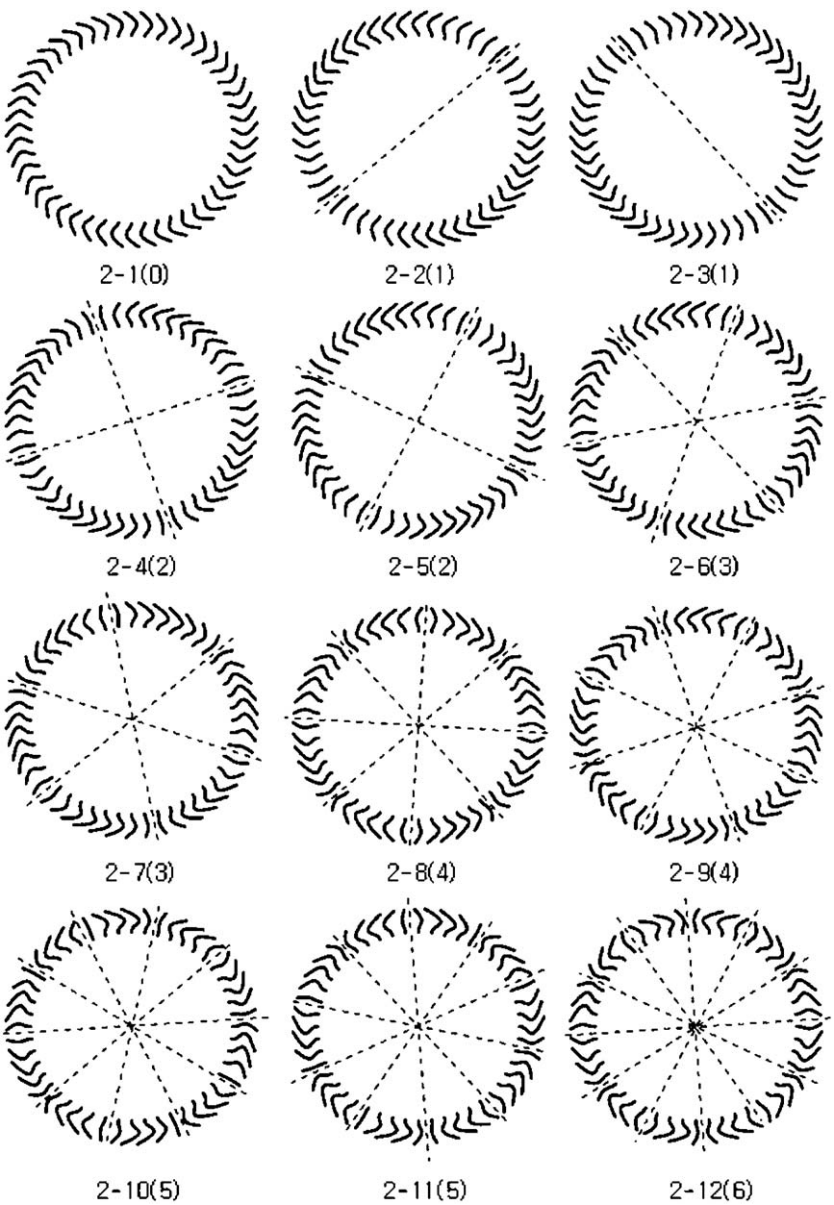

Fig. 6. The lowest 12 mode shapes of the second set of natural frequencies.

3. Numerical results

The multi-packet blade system analyzed in this section has eight packets that consist of 48 blades in total, so each packet consists of six blades. To obtain the numerical results, five assumed modes, which are the bending mode functions of a cantilever beam, are employed for each blade. In all, 240 mode functions are employed for the analysis. With the number of mode functions, well converged modal characteristics of the system can be obtained.

To verify the accuracy of the proposed model, modal analysis results of the multi-packet blade system are obtained by using a finite element code (see Ref. [25]). The beam element of the FE code is BEAM 3node 189 which is used for a tapered beam. Since 10 beam elements are used for a blade, 480 beam elements are used for the total blade system. The FE results

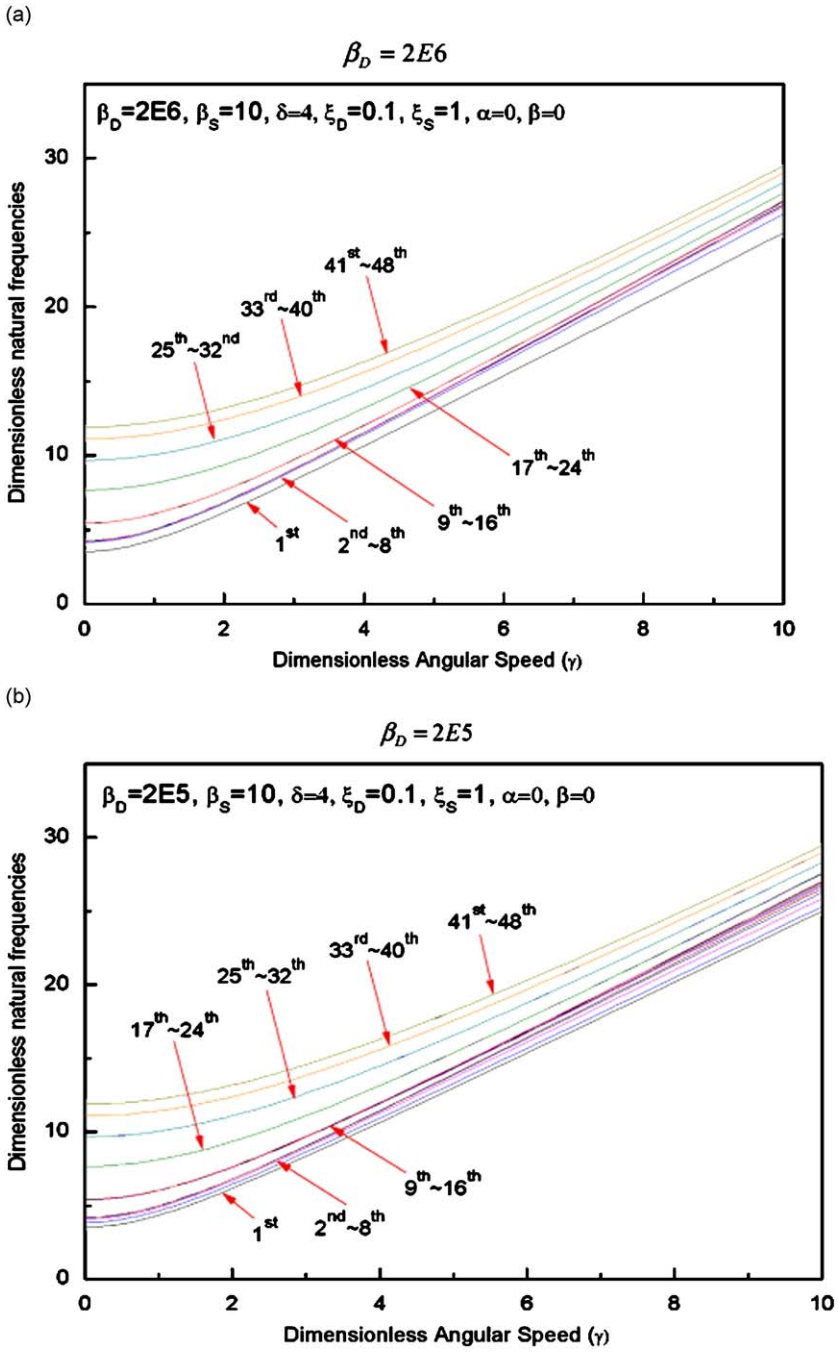

Fig. 7. The effect of disc stiffness variation on the first set natural frequencies: (a) $\beta_D = 2E6$; (b) $\beta_D = 2E5$.

are compared to those obtained with the proposed model. As shown in Table 2, lowest 16 natural frequencies are compared with a set of typical parameter values ($\gamma = 5,\ \delta = 0,\ \beta_D = 2E6,\ \beta_S = 10,\ \xi_D = 0.1,\ \xi_S = 1.0$). The reason why the hub radius ratio is given as zero is that the direction of the shroud spring force cannot be perpendicular to the blade in ANSYS model while it is so in the real system. To reduce the modeling error of the ANSYS model, the radius is given as zero here. Two cases of thickness taper ratios ($\alpha = 0, \alpha = 0.5$) and width taper ratios ($\beta = 0, \beta = 0.5$) are employed to obtain the 4 sets of results. The results obtained with the proposed model are in good agreement with those obtained with the finite element code. The maximum relative difference between the two sets of results is less than 1%.

Fig. 4 shows the dimensionless natural frequencies versus the dimensionless angular speed of the system. All the values of the dimensionless parameters used for the numerical analysis are given in the figure. These are typical values for a multi-

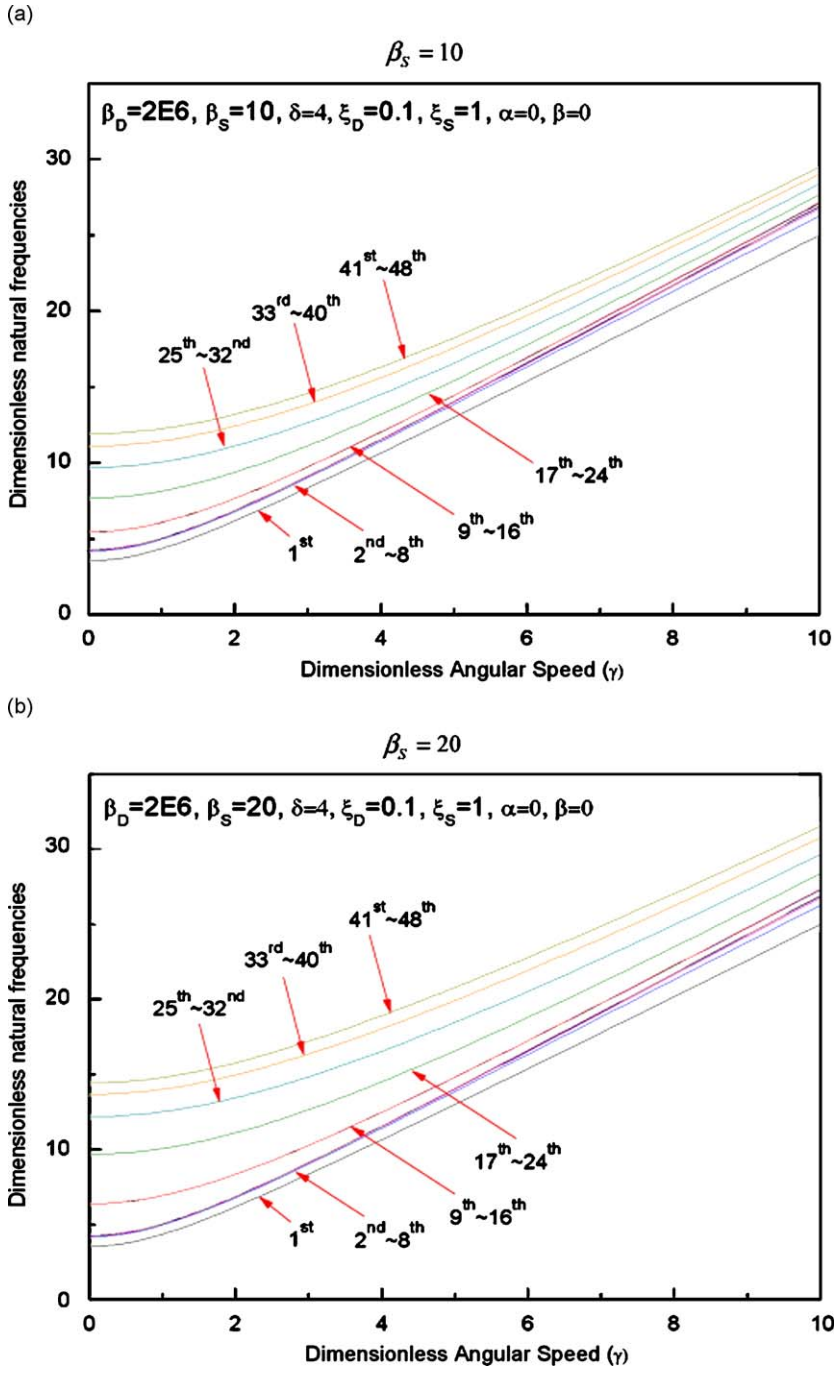

Fig. 8. The effect of shroud stiffness variation on the first set natural frequencies: (a) $\beta_S = 10$; (b) $\beta_S = 20$.

packet blade turbine system. Since five mode functions are employed for each beam, one can obtain 240 natural frequencies (5×48) with the model. Only 144 natural frequencies (3×48) are exhibited in this figure. Three sets of natural frequencies are shown in the figure. Each set consists of 48 natural frequencies. As shown in the figure, all the natural frequencies increase as the angular speed increases. The lowest natural frequencies in the three sets are same as the lowest three natural frequencies of a single blade. Due to the stiffness coupling effects caused by the disc and the shroud flexibilities, the 48 natural frequencies in each set have distinct values in general.

Figs. 5 and 6 show some mode shapes of the first and the second sets of natural frequencies. Nodal diameters of the first 12 mode shapes of the two sets are shown in the figures. The maximum number of nodal diameters is half the number of

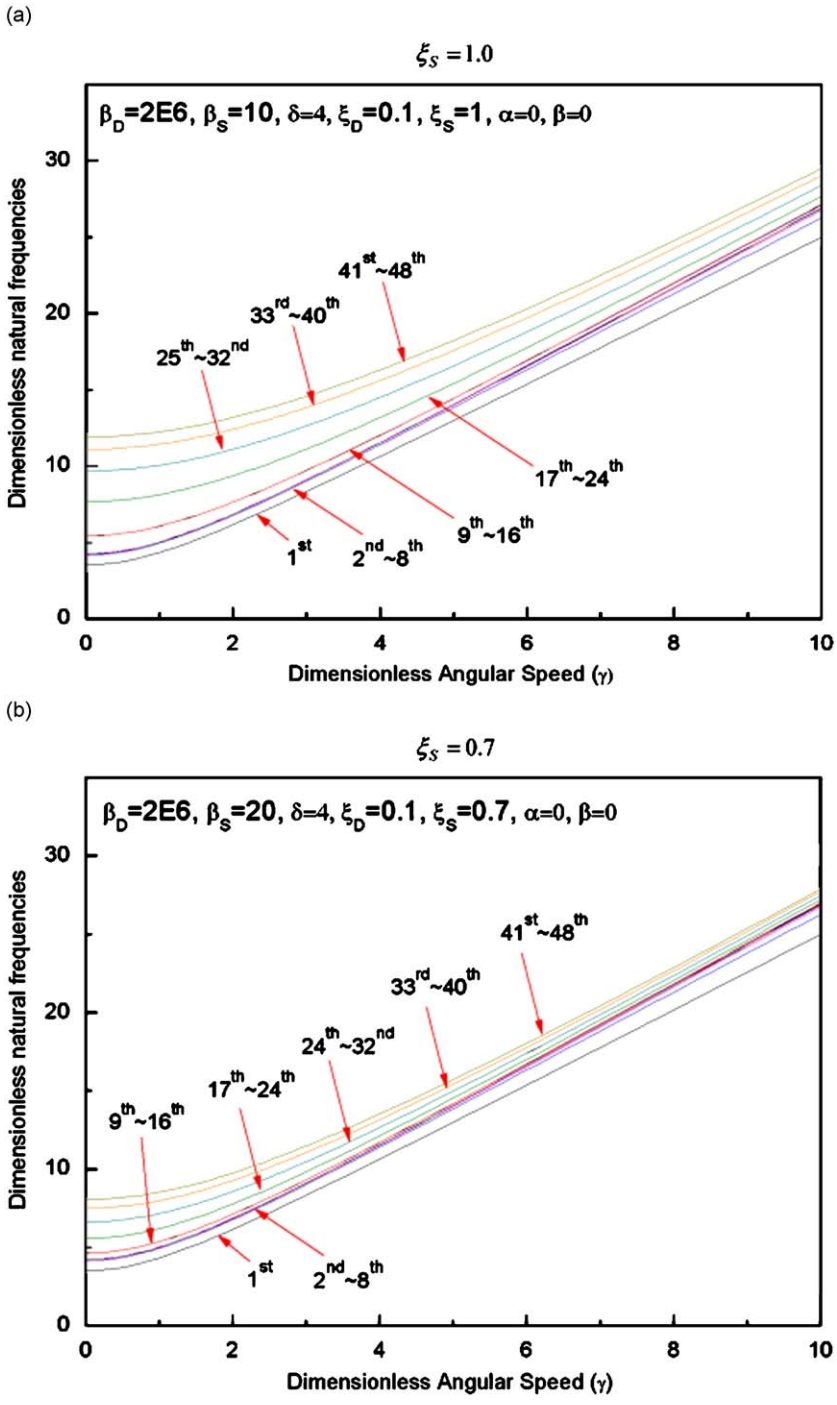

Fig. 9. The effect of shroud location variation on the first set natural frequencies: (a) $\xi_S = 1.0$; (b) $\xi_S = 0.7$.

blades when the number of the blades is even. For a system having an odd number of blades, the maximum nodal diameter is (number of blades−1)/2. The integer numbers $m-n(k)$ shown in the figures indicate the set number, the natural frequency number in the set, and the number of nodal lines of the mode, respectively. There always exist two natural frequencies for a number of nodal lines in each set (except the first and the last natural frequencies). The first mode in each set always has zero nodal lines.

Fig. 7 shows the first set of natural frequencies versus the angular speed. The variation effect of the dimensionless disc stiffness β_D on the natural frequencies is shown in Fig. 7. Comparing the results shown in Fig. 7(a) and (b), it can be easily found that the natural frequencies are rarely influenced by the variation of β_D even though the value of β_D employed to

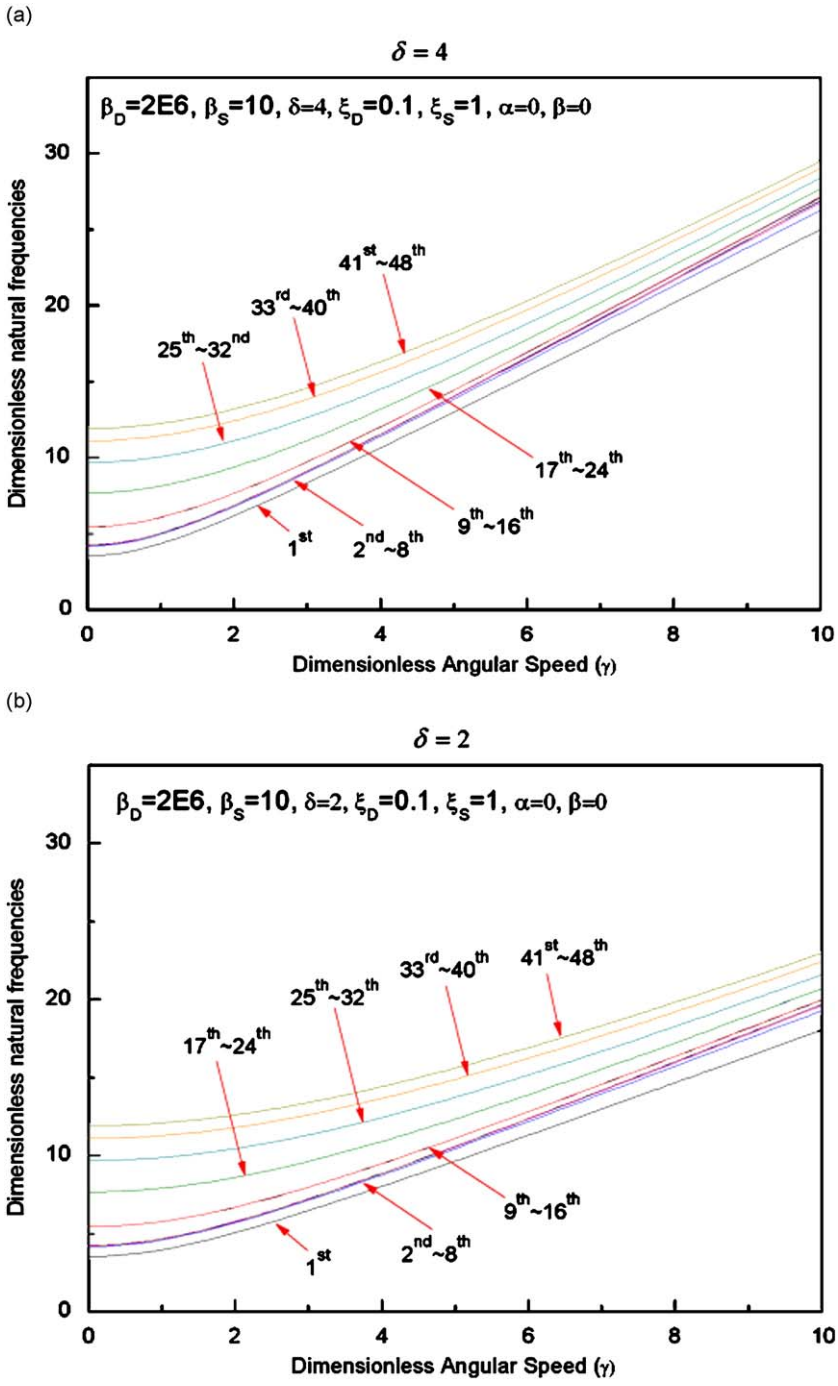

Fig. 10. The effect of hub radius variation on the first set natural frequencies: (a) $\delta = 4$; (b) $\delta = 2$.

obtain the results in Fig. 7(b) is one-tenth of that in Fig. 7(a). One can observe that the 48 frequency loci are densely populated at seven locations which are represented by identical color lines. It is interesting to see that the second lowest group gets sparse as β_D decreases.

Fig. 8 shows the variation effect of the dimensionless shroud stiffness β_S on the natural frequencies of the first set. Fig. 8(b) shows that the lowest frequency is not influenced by the variation effect, but the higher frequencies are

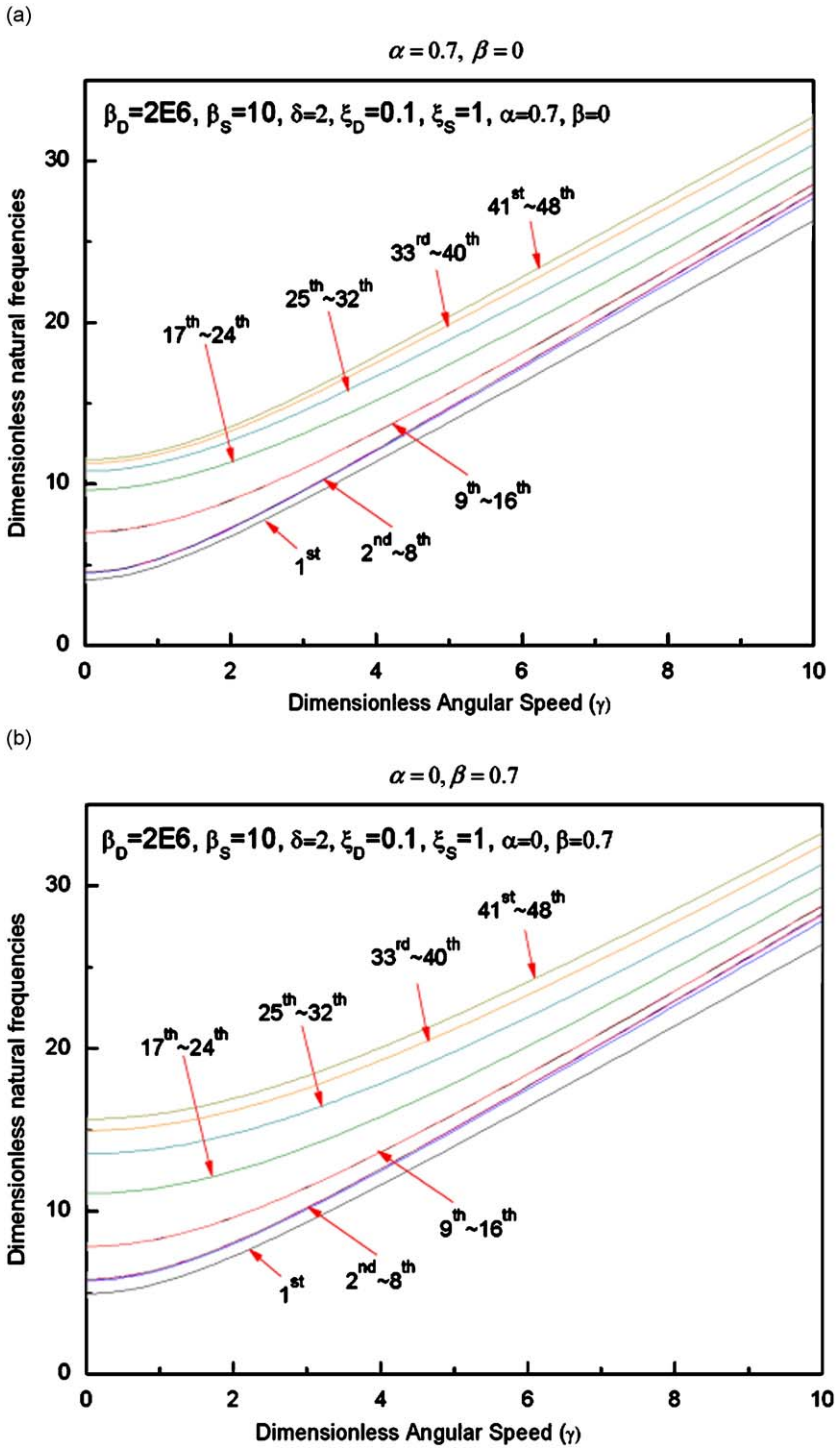

Fig. 11. Separate variation effects of taper parameters on the first set natural frequencies: (a) $\alpha = 0.7$, $\beta = 0$; (b) $\alpha = 0$, $\beta = 0.7$.

significantly influenced by the variation of β_S. The existing range of the natural frequencies that belong to the first set becomes wider as the value of β_S increases.

Fig. 9 shows the variation effect of the dimensionless shroud location ξ_S on the natural frequencies of the first set. As shown in the figure, the lowest frequency is not influenced by the variation of ξ_S, but the higher frequencies are significantly influenced by the variation. As shown in Fig. 9(b), the existing range of the natural frequencies that belong to the first set becomes narrower as the value of ξ_S decreases. Compared to the previous results shown in Fig. 8, the variation effect of ξ_S on the higher natural frequencies is more significant than that of β_S.

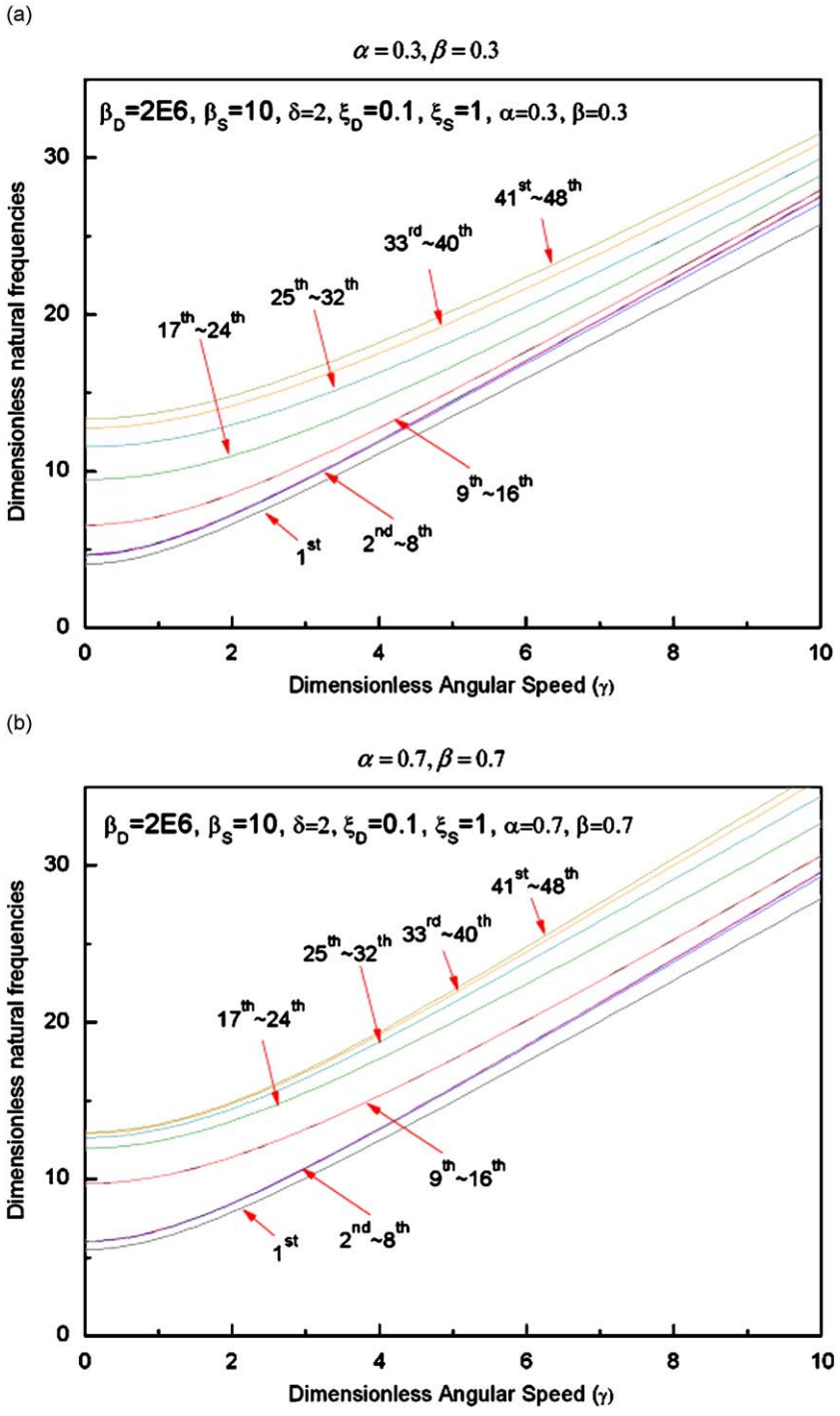

Fig. 12. Simultaneous variation effects of taper parameters on the first set natural frequencies: (a) $\alpha = 0.3$, $\beta = 0.3$; (b) $\alpha = 0.7$, $\beta = 0.7$.

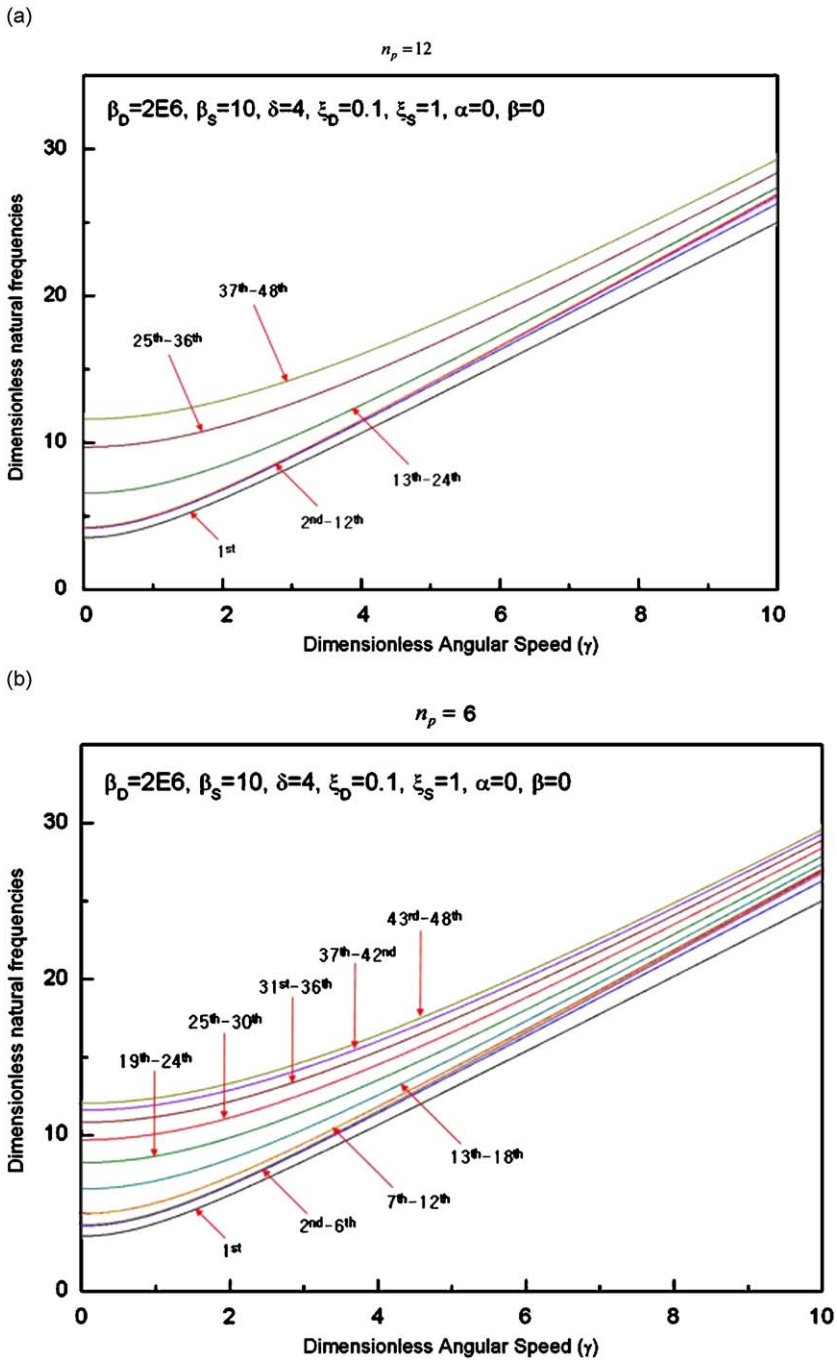

Fig. 13. The effect of number of packets on the first set natural frequencies: (a) $n_p = 12$; (b) $n_p = 6$.

Fig. 10 shows the variation effect of the dimensionless disc radius δ on the natural frequencies of the first set. As can be inspected, the natural frequencies are not influenced by the variation effect when γ is equal to 0. However, the increasing rates of natural frequencies are significantly influenced by the disc radius ratio δ.

Fig. 11 shows separate variation effects of the taper parameters α and β on the first set natural frequencies. Comparing to the results of Fig. 10(a), the slopes of the natural frequency loci become stiffer as the two taper parameters increase up to 0.7. An interesting fact one can observe from Fig. 11(b) is that the gaps among the natural frequency loci increase significantly as the width taper ratio increases up to 0.7. Fig. 12 shows the simultaneous variation effects of the taper parameters α and β on the first set natural frequencies. As the taper parameters increase simultaneously, the slopes of the

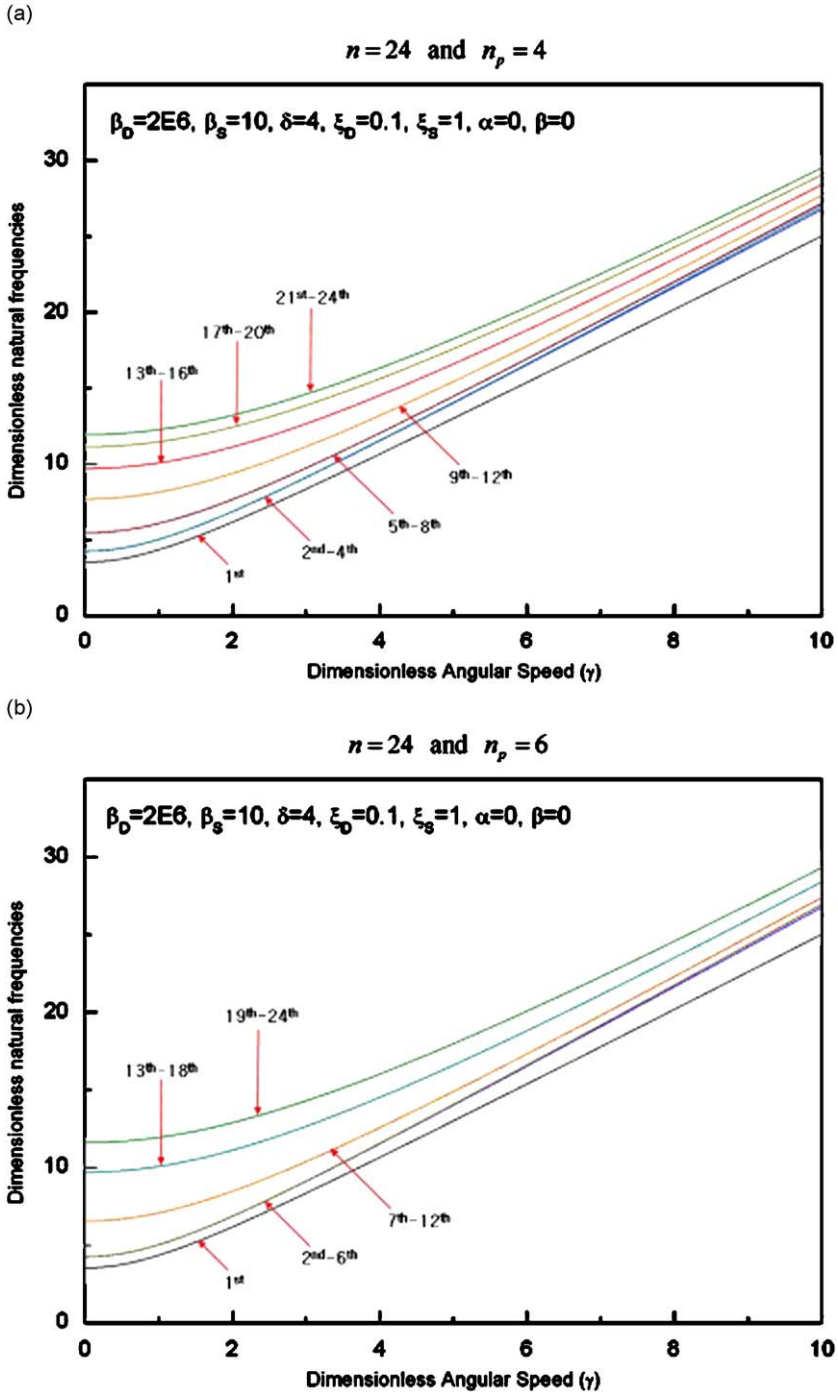

Fig. 14. The effect of total number of blades along with number of packets: (a) $n = 24$ and $n_p = 4$; (b) $n = 24$ and $n_p = 6$.

natural frequency loci are getting stiffer. One can also observe that the gap between the lowest natural frequency locus and the highest natural frequency locus becomes uniform as the two taper ratios increase.

Fig. 13 shows the variation effect of the number of packets n_p on the natural frequencies of the first set. Compared to the previous results (shown in Fig. 10(a)) for which $n_p = 8$ is employed, the highest frequency is slightly influenced by the variation of n_p. However, it can be observed that the distribution pattern of the 48 natural frequencies has changed as the number of packets n_p varies. The 48 natural frequencies are now populated at five locations in Fig. 13(a) and at nine locations in Fig. 13(b). In fact, the number of densely populated locations is equal to $n/n_p + 1$. Therefore, if the number of densely populated locations of natural frequencies needs to be minimized, the number of packets has to be increased.

Fig. 14 shows the results in which the blades employed for the numerical analysis are equal to 24. Even if the total number of blades is decreased, the natural frequency distribution pattern remains almost unchanged. Again, the number of densely populated locations is equal to $n/n_p + 1$.

4. Conclusion

In the present work, a modeling method for the modal analysis of a rotating multi-packet blade system is proposed. The effects of angular speed, disc flexibility, shroud flexibility, shroud location, disc radius, thickness and width taper ratios of the beam cross section, number of packets and total number of blades on the modal characteristics of the system are investigated. The disc flexibility and the total number of blades have little influence on the modal characteristics of the system when typical values of the parameters are employed. Both the location and the stiffness of the shroud affect the modal characteristics significantly, while the former parameter has more influence than the latter. As the disc radius increases, the increasing slopes of the natural frequency loci become stiffer. The thickness and width taper parameters may also affect the modal characteristics significantly. Variations of the two taper parameters affect the slopes of the natural frequency loci and the gaps among the loci. Lastly the number of densely populated locations of a set of natural frequencies is equal to the number of blades divided by the number of packets plus one.

Acknowledgment

This work was supported by the research fund of Hanyang University (HY-2007-I), for which authors are grateful.

References

[1] R. Southwell, F. Gough, The free transverse vibration of airscrew blades, *British A.R.C. Reports and Memoranda* 766 (1921).
[2] M. Schilhansl, Bending frequency of a rotating cantilever beam, *Journal of Applied Mechanics, Transactions of the ASME* 25 (1958) 28–30.
[3] A.W. Leissa, Vibration aspects of rotating turbomachinery blades, *Applied Mechanics Reviews* 34 (1981) 629–635.
[4] J.S. Rao, Turbomachine blade vibration, *Shock Vibration Digest* 19 (1987) 3–10.
[5] C.D. Eick, M.P. Mignolet, Vibration and buckling of flexible rotating beams, *AIAA Journal* 33 (3) (1995) 528–538.
[6] J.S. Huang, R.F. Fung, C.R. Tseng, Dynamic stability of a cantilever beam attached to a translational/rotational base, *Journal of Sound and Vibration* 224 (2) (1999) 221–242.
[7] H. Dicken, Vibration control of a rotating Euler–Bernoulli beam, *Journal of Sound and Vibration* 232 (3) (2000) 541–551.
[8] Y. Yang, C. Ju, C.K. Soh, Analytical and semi-analytical solutions for vibration control of a cantilevered column using a piezoelectric actuator, *Smart Materials and Structures* 12 (2003) 193–203.
[9] T.R. Kane, R.R. Ryan, A.K. Banerjee, Dynamics of a cantilever beam attached to a moving base, *Journal of Guidance, Control, and Dynamics* 10 (2) (1987) 139–151.
[10] H.H. Yoo, R.R. Ryan, R.A. Scott, Dynamics of flexible beams undergoing overall motions, *Journal of Sound and vibration* 181 (1995) 261–278.
[11] H.H. Yoo, S.H. Shin, Vibration analysis of rotating cantilever beams, *Journal of Sound and Vibration* 212 (1998) 807–828.
[12] G.H. Zhang, Z.S. Liu, H.H. Yoo, In-plane vibration analysis of cantilevered circular arc beams undergoing rotational motion, *Journal of Mechanical Science and Technology* 22 (2008) 113–119.
[13] W.H. Huang, Free and forced vibration of closely coupled turbomachinery blades, *AIAA Journal* 19 (1981) 918–924.
[14] D.J. Ewins, M. Imregun, Vibration modes of packeted bladed disks, *Journal of Vibration, Acoustics, Stress, and Reliability in Design, Transactions of the ASME* 106 (1984) 175–180.
[15] M. P. Singh, D. M. Schiffer, Vibrational characteristics of packeted bladed discs, *ASME Paper* No. 82-DET-137 (1982) 1–8.
[16] T. Tomioka, Y. Kobayashi, G. Yamada, Analysis of free vibration of rotating disk-blade coupled systems by using artificial springs and orthogonal polynomials, *Journal of Sound and Vibration* 191 (1) (1996) 53–73.
[17] H.H. Yoo, J.H. Park, J. Park, Vibration analysis of rotating pre-twisted blades, *Computers and Structures* 79 (2001) 1811–1819.
[18] H.H. Yoo, J.Y. Kwak, J. Chung, Vibration analysis of rotating pre-twisted blades with a concentrated mass, *Journal of Sound and Vibration* 240 (5) (2001) 891–908.
[19] T.R. Kane, D.A. Levinson, *Dynamics: Theory and Application*, McGraw-Hill, New York, 1985.
[20] A. Chatterjee, The short-time impulse response of Euler–Bernoulli beams, *ASME Journal of Applied Mechanics* 71 (2004) 208–218.
[21] S.K. Sinha, Non-linear dynamic response of a rotating radial Timoshenko beam with periodic pulse loading at the free-end, *International Journal of Non-linear Mechanics* 40 (2005) 113–149.
[22] Y.L. Lau, R.C.K. Leung, R.M.C. So, Vortex-induced vibration effect on fatigue life estimate of turbine blades, *Journal of Sound and Vibration* 307 (2007) 698–719.
[23] Z. Hu and G. Zha, Parallel computation of forced vibration for compressor cascade, Collection of Technical Papers, *44th AIAA Aerospace Sciences Meeting* 10 (2006) 7521–7534.
[24] H.A. Chuang, J.M. Verdon, A non-linear numerical simulator for three-dimensional flows through vibrating blade rows, *Journal of Turbomachinery* 121 (2) (1999) 348–357.
[25] ANSYS, User's Manual, Structural Analysis Guide, ANSYS Inc, 1998.